Tunable Constant-Bandwidth Substrate-Integrated Bandstop Filters

Mark D. Hickle, *Member, IEEE*, and Dimitrios Peroulis, *Fellow, IEEE*

***Abstract*— A new method for designing tunable bandstop filters with constant fractional and absolute bandwidths (ABWs) is presented. The constant bandwidth is achieved through a new coupling structure, which is passive and consists only of coupling elements and transmission lines. Its theory of operation is presented, and design principles and tradeoffs are examined in detail. Several prototype filters are fabricated and measured to demonstrate the performance and versatility of this method. An octave-tunable filter with less than 12% fractional bandwidth variation is demonstrated, along with an octave-tunable filter with 12.3% variation in ABW variation, a filter with a 50% tuning range and less than 4% variation in ABW, and a four-pole octave-tunable filter with less than 4% variation in its 10-dB ABW. These results represent state-of-the-art performance when compared to other constant-bandwidth bandstop filters at frequencies higher than those compatible with lumped-element filters.**

***Index Terms*— Filters, microwave filters, notch filters, resonator filters, tunable circuits and devices.**

I. Introduction

TUNABLE bandstop filters have been the focus of many research endeavors in recent years due to their ability to dynamically suppress signals by many orders of magnitude with a high degree of selectivity. They can be cascaded with bandpass filters in order to provide extremely high rejection [1], [2], or can be used without preselect bandpass filters to realize very wideband receivers with the ability to selectively reject undesired signals.

Though many excellent examples of tunable bandstop filters have been demonstrated, most suffer from large variations in bandwidth when tuned over wide frequency ranges. A survey of published tunable bandstop filters reveals this limitation. In [3], a bandstop filter which has a 0.65–1.65-GHz tuning range and a 1.2%–3.2% fractional bandwidth (FBW) is presented. An 8.6%–11.3% FBW is seen in [4], which is a bandstop filter with a 1.3–2.3-GHz tuning range. The filter in [5] experiences a 4%–5.9% FBW over an 8.9–11.3-GHz tuning range, and the filter in [6] also experiences a 1.6%–4.2% FBW with slightly over an octave tuning range.

The frequency variation of bandwidth is related to the external coupling structures which connect a filter's resonators to its signal path. The FBW of a first-order lossless bandstop filter consisting of a parallel resonator coupled to a source-to-load transmission line with an external coupling element of magnitude K_0 can be shown to depend only on the external coupling [7]

$$\mathrm{FBW}_{3\mathrm{dB}} = \frac{K_0^2}{2}. \tag{1}$$

Though factors such as finite unloaded quality factor and non $-90°$ lengths of transmission lines complicate analytical expressions for the bandwidths of higher order bandstop filters, they are still primarily determined by the strength of the external coupling. Typical microwave coupling structures used to realize external couplings in bandstop filters include coupled microstrip lines, lumped capacitors, or inductors, and apertures in cavities. Coupling structures which rely on a certain geometry to provide the desired coupling coefficients, such as coupled sections of microstrip lines or apertures in cavities, have frequency variation because the electrical size of the structure increases as frequency is increased. Lumped-element coupling structures such as capacitors or inductors exhibit frequency-dependent reactances which lead to changes in coupling magnitude.

It is usually even more challenging to maintain constant absolute bandwidth (ABW) across a wide tuning range because ABW is equal to $\mathrm{FBW} \cdot f_0$, where f_0 is the center frequency of the filter. Even with a perfectly constant FBW, the ABW of a filter will double when tuned over an octave tuning range. To maintain constant ABW, the FBW must decrease linearly with frequency, which requires the external coupling coefficient to be inversely proportional to the square root of frequency.

Several methods for addressing the problem of bandwidth variation have been presented. In [8] and [9], lumped-element absorptive bandstop filters are implemented with inductive admittance inverters which, when combined with capacitively tuned resonators, provide fairly constant ABW over more than an octave tuning range. Due to the use of lumped-element inductors and capacitors, however, this method is only applicable for frequencies less than approximately 2 GHz.

Another method for maintaining constant ABW is to realize the external coupling with an electrically long section of coupled transmission lines. The length of the coupling section can be optimized to blend electric and magnetic coupling, and

Manuscript received December 13, 2016; revised April 21, 2017 and June 27, 2017; accepted July 28, 2017. Date of publication August 30, 2017; date of current version January 4, 2018. The work of M. D. Hickle was supported by the National Defense Science and Engineering Graduate Fellowship through the Department of Defense. *(Corresponding author: Mark D. Hickle.)*

M. D. Hickle was with the School of Electrical and Computer Engineering and the Birck Nanotechnology Center, Purdue University, West Lafayette, IN 47907 USA. He is now with BAE Systems, Inc., Merrimack, NH 03054 USA (e-mail: mark.hickle@ieee.org).

D. Peroulis is with the School of Electrical and Computer Engineering and the Birck Nanotechnology Center, Purdue University, West Lafayette, IN 47907 USA (e-mail: dperouli@purdue.edu).

Color versions of one or more of the figures in this paper are available online at http://ieeexplore.ieee.org.

Digital Object Identifier 10.1109/TMTT.2017.2740170

the opposite frequency dependencies of these two types of coupling can partially compensate for each other, yielding a fairly constant bandwidth. Examples of this method can be found in [10] and [11]. This method works well, as [10] demonstrated a 92% center frequency tuning range with only 24% variation in 3-dB bandwidth. However, this method is only applicable to microstrip or other electrically long resonators which can use both electric and magnetic coupling.

A third method for realizing constant-bandwidth filters is to utilize tunable coupling elements, so that the coupling can be reduced at higher frequencies in order to maintain constant ABW. In [7] and [12], microstrip resonators loaded with varactors on each end are used. By differentially tuning the varactors, the voltage and current distributions on the resonator can be modified, which tunes the external coupling coefficient and thus the filter's bandwidth. Specifically, [12] demonstrates a constant 100-MHz 3-dB bandwidth over a 1.2–1.6-GHz center frequency tuning range. Using the same method, the filter in [7] has a 3-dB bandwidth which can be held constant over a 0.67–1-GHz tuning range. In [13], substrate-integrated waveguide cavity resonators are coupled to a through-line with varactors, which allows the filter to maintain a constant 83-MHz 3-dB bandwidth across a 0.77–1.25-GHz tuning range. Using tunable coupling elements allows tunable filters to maintain constant bandwidth, but it increases control complexity due to the additional tuning elements, and also decreases the filter's linearity and adds additional loss.

Until recently, there was no way to passively control the bandwidth variation of high-Q tunable evanescent-mode cavity resonators. The lumped-element coupling method of [8] is not compatible with this type of resonator, particularly at high frequencies where lumped-element components are very lossy. The electric field is concentrated into a very small portion of resonator's volume, while the magnetic field is fairly evenly distributed throughout the volume of the resonator, making it difficult to simultaneously realize both electric and magnetic coupling. Thus, the method used in [11] cannot be used. Tunable coupling elements can be used, as in [13], but it is often preferable to avoid the additional tuning elements introduced by tunable coupling.

A new coupling method for bandstop filters was recently presented by Hickle and Peroulis [14], which for the first time allowed control over the bandwidth of tunable bandstop filters utilizing evanescent-mode cavity resonators. This paper presented preliminary results of this method, consisting of a tunable bandstop filter which had only 27% variation in its 3-dB ABW over an octave center-frequency tuning range—an 80% reduction in bandwidth variation compared to the typical method of coupling for these filters.

This paper builds upon this work by investigating this new bandwidth control method in greater detail and presenting new results which have improved performance over and go beyond the scope of the results in [14]. Specifically, five *S*- to *C*-band filters are designed, implemented, and measured in order to demonstrate the efficacy and versatility of this method.

1) A two-pole constant-FBW filter with an octave tuning range and only 12% variation in 3-dB FBW.
2) A two-pole constant-ABW filter with an octave tuning range and only 12.3% variation in its ABW—a 55% improvement over [14].
3) A two-pole constant-ABW filter with a 50% tuning range and only 3.8% variation in ABW.
4) A constant-ABW octave-tunable four-pole filter which can maintain a constant 10-dB ABW, limited only by tuning and measurement accuracy.
5) An uncompensated tunable bandstop filter designed using the traditional coupling method, in order to show the benefit provided by this new coupling method.

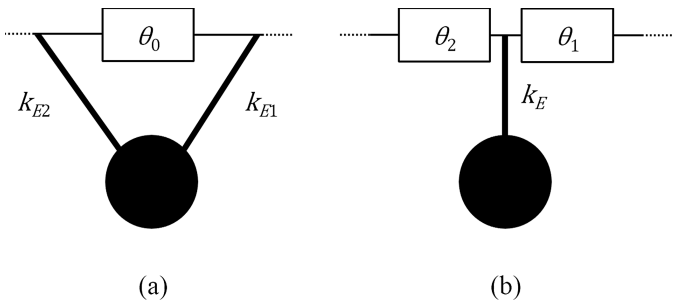

Fig. 1. (a) Twice-coupled resonator topology for constant bandwidth. (b) Equivalent circuit of (a).

By comparing the constant-bandwidth filters to the control filter which is designed without the constant-bandwidth coupling method, it is shown that over an octave tuning range the new coupling method can reduce the FBW variation by up to 86%, and can reduce the ABW variation by up to 95%.

In addition to the new results presented, this paper investigates the optimal performance as well as limitations of this method. It also presents background theory and design considerations, such as the relationship between tuning range and bandwidth variation, and the effects of coupling sign and transmission line length on bandwidth variation. It is shown that in addition to providing greatly reduced bandwidth variation, this coupling method also reduces the phase variation of the transmission line between the two resonators of a two-pole bandstop filter. This helps maintain the symmetry of the filter's transfer function over wide tuning ranges.

This paper is organized as follows. Section II develops the background theory and design space of the coupling structure introduced in [14], presenting design principles and design tradeoffs. Section III details the design of constant-bandwidth filters based on evanescent-mode cavities using the new coupling method. Section IV presents the measured results of the designed filters, and Section V concludes the work.

II. Constant-Bandwidth Coupling Concept

The coupling topology studied in this paper is shown in Fig. 1(a). This circuit was first introduced in [7] in order to realize intrinsically switched bandstop filters, and was proposed in [14] for the purpose of constant-bandwidth filters.

It can be shown that the circuit of Fig. 1(a), consisting of a resonator coupled twice to a through-line of length θ_0 with external coupling elements k_{E1} and k_{E2}, is equivalent to the

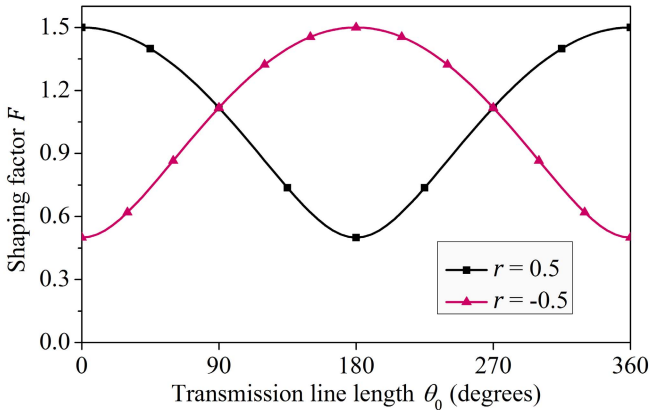

Fig. 2. Frequency variation of the shaping factor F, which modifies the frequency dependence of the individual coupling coefficients.

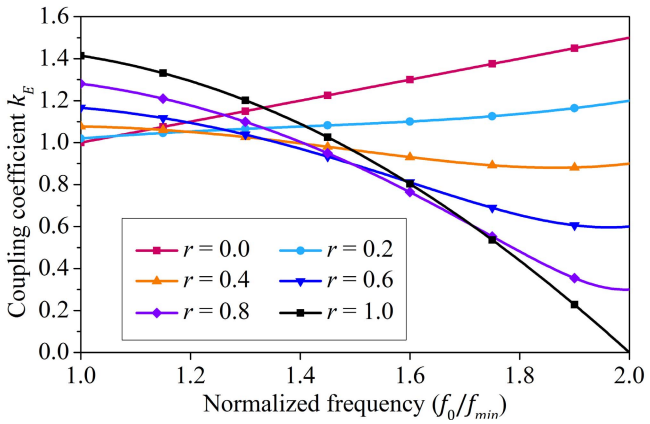

Fig. 3. Frequency variation of the coupling coefficient k_E for various values of the coupling ratio r. $\theta_0 = 180°$ at a normalized frequency of 2.

circuit of Fig. 1(b), which comprises a resonator coupled to a through-line with only a single coupling element k_E, followed and preceded by transmission lines of lengths θ_1 and θ_2 [7]. The coupling elements are modeled as admittance inverters, as described in [7]. The equations relating the expressions in the equivalent circuit to those of the original circuit are

$$k_E = \sqrt{k_{E1}^2 + k_{E2}^2 + 2k_{E1}k_{E2}\cos(\theta_0)} \tag{2}$$

$$\theta_1 = \frac{1}{2}\left(\pi - \arg\left(-\frac{\frac{k_{E1}}{k_{E2}} + e^{-j\theta_0}}{\frac{k_{E1}}{k_{E2}} + e^{j\theta_0}}\right)\right) \tag{3}$$

$$\theta_2 = \theta_0 - \theta_1. \tag{4}$$

If the two coupling elements k_{E1} and k_{E2} have approximately the same frequency dependence but one is a fraction of the other, for example

$$k_{E2} \approx r k_{E1} \tag{5}$$

where r is a constant, then (2) can be approximated as

$$k_E \approx k_{E1} F \tag{6}$$

$$F = \sqrt{1 + r^2 + 2r\cos(\theta_0)}. \tag{7}$$

We now see that the total equivalent coupling coefficient is equal to the original coupling coefficient k_{E1} multiplied by a shaping factor F, which has a sinusoidal frequency dependence since the electrical length of the transmission line θ_0 is proportional to frequency. The frequency dependence of the shaping factor F is shown in Fig. 2. It can be seen that when the two coupling coefficients have the same sign ($r > 0$), F decreases with frequency for $0° < \theta_0 < 180°$ and increases with frequency for $180° < \theta_0 < 360°$. Conversely, when the two coupling coefficients have opposite sign ($r < 0$), the opposite trend is observed: F has a positive frequency dependence for $0° < \theta_0 < 180°$ and a negative frequency dependence for $180° < \theta_0 < 360°$. The regions where F has negatively sloped frequency dependence can be used to at least partially compensate for the positive frequency dependence inherent to the original coupling structure.

To show how this method can realize constant-coupling coefficients for constant-FBW filters and coupling coefficients which decrease with frequency for constant-ABW filters,

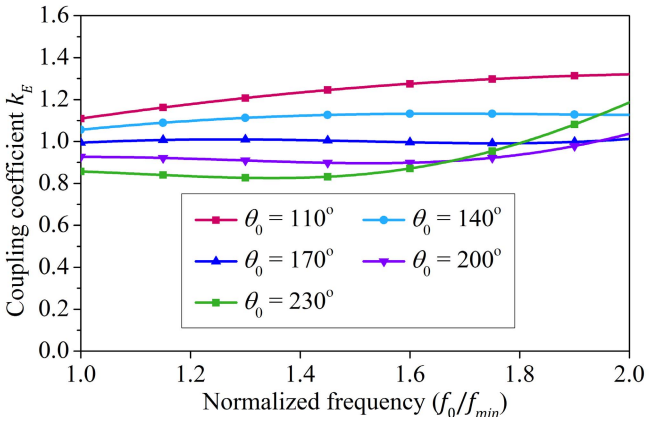

Fig. 4. Frequency variation of k_E for various values of transmission line length θ_0, with $r = 0.3$. The values of θ_0 are defined at $f_{\max}$.

we will use a frequency-dependent model for the coupling coefficients and investigate how the various design parameters affect the frequency variation of the composite coupling coefficient k_E. In the rest of Section II, k_{E1} is defined such that it has a value of 1 at the resonator's minimum tuned frequency $f_{\min}$ and increases by 50% over an octave tuning range

$$k_{E1} = 1 + 0.5\left(\frac{f_0}{f_{\min}} - 1\right). \tag{8}$$

This is a first-order approximation of the frequency dependence observed in typical coupling structures, and we will see in Section III that it models the frequency dependence of the utilized coupling structure fairly well.

The coupling coefficient k_E is plotted versus normalized center frequency ($f_0/f_{\min}$) for several values of r in Fig. 3. It can be seen that when r is zero, k_E is the same as that of a single coupling element, and increases by 50% over an octave tuning range. As r increases, k_E is increased at lower frequencies and reduced at higher frequencies, becoming zero at the frequency at which θ_0 is 180° when $r = 1$.

The dependence of coupling variation on the length of the transmission line θ_0 is shown in Fig. 4. The stated values of θ_0 are defined at the maximum tuned center frequency $f_{\max}$, which in this case is a normalized frequency of 2. It can

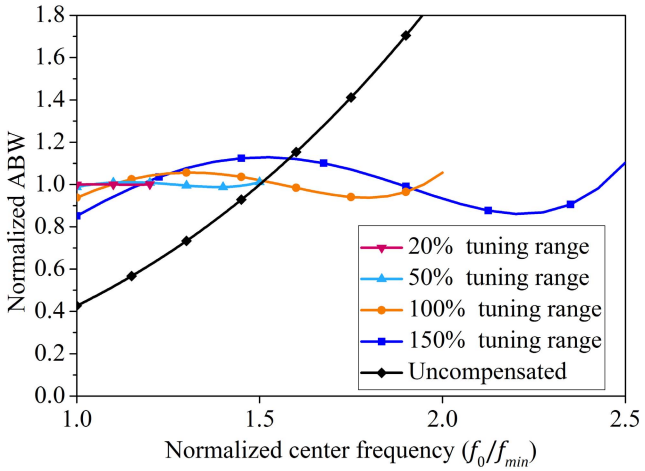

Fig. 5. ABW variation for different tuning ranges. The coupling ratio r is positive, and the values of r and θ_0 can be found in Fig. 7(b).

be seen that for values of θ_0 less than 170°, the coupling coefficient has a concave-down shape, whereas it is concave-up for lengths of θ_0 greater than 170°. For the specific frequency dependence of the coupling coefficient used in this example, choosing $\theta_0 = 170°$ at $f_{\max}$ and $r = 0.28$ results in a nearly constant coupling coefficient as needed for constant FBW, and choosing $\theta_0 = 180°$ and $r = 0.6$ causes the coupling coefficient to decrease with frequency as required for constant ABW.

Though nearly constant, the resulting coupling coefficient has a slight sinusoidal frequency variation which in general has a single local maximum and a single local minimum. The frequency variation of k_E can be minimized (to obtain constant FBW) by choosing the values of r and θ_0 such that both the global and local maxima are equal, and the global and local minima are equal, as seen in Figs. 5 and 8. Designing for constant ABW is nearly the same as designing for constant FBW, except that the quantity $k_E^2 \cdot f_0$ (which is proportional to ABW) should be minimized instead of k_E. This optimization of r and θ_0 can either be done manually, using the trends shown in Figs. 3 and 4, or can be accomplished with an optimization algorithm.

One key characteristic of the proposed method is that its topology is generic, and can in principle be applied to any tunable resonator technology. This is in contrast to the existing constant-bandwidth methods described in Section I, which are applicable only to specific technologies.

A. BW Variation Versus T-Line Length and Tuning Range

The shaping factor F can have a negative slope with respect to frequency over a wide range of frequencies, and thus is able to reduce the amount of bandwidth variation over wide tuning ranges. However, it can be seen that F is much more linear over narrow ranges of θ_0 (in the neighborhood of $\theta_0 = 90°$ when r is positive and $\theta_0 = 270°$ when r is negative), and it is thus expected that this method will be even more effective when utilized over narrow tuning ranges. In general, the amount of reduction in bandwidth variation is a nonlinear

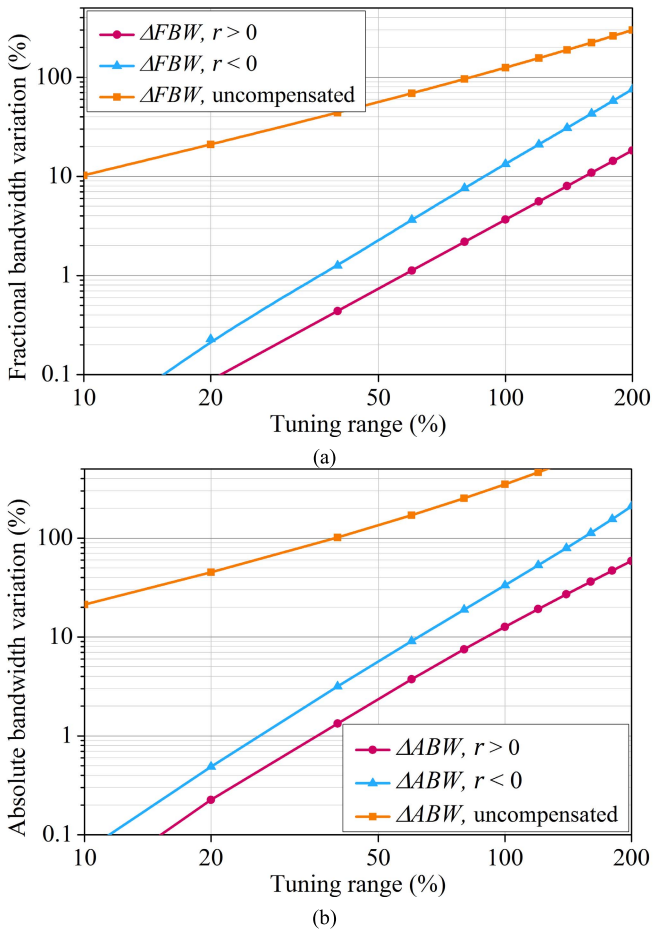

Fig. 6. (a) Minimum ABW variation and (b) minimum FBW variation as a function of center frequency tuning range.

function of the tuning range over which the bandwidth variation is optimized. To show this, the transmission line length θ_0 and coupling ratio r were optimized in order to provide minimum bandwidth variation, for a variety of tuning ranges.

The resulting ABW variation curves are shown in Fig. 5. As expected, for all tuning ranges the bandwidth variation is significantly reduced compared to the uncompensated case. However, as the tuning range decreases, the bandwidth variation reduces dramatically and can become nearly constant for small tuning ranges.

The optimized fractional and ABW variations (ΔFBW and ΔABW, respectively) are plotted as a function of tuning range in Fig. 6(a) and (b). The quantities ΔFBW, ΔABW, and tuning range are calculated as

$$\Delta\text{FBW} = 100 \cdot \left(\frac{\max\ (\text{FBW})}{\min\ (\text{FBW})} - 1 \right) \tag{9}$$

$$\Delta\text{ABW} = 100 \cdot \left(\frac{\max\ (\text{ABW})}{\min\ (\text{ABW})} - 1 \right) \tag{10}$$

$$\text{Tuning range} = 100 \cdot \left(\frac{f_{\max}}{f_{\min}} - 1 \right). \tag{11}$$

Fig. 6(a) and (b) shows the degree to which the proposed method can reduce bandwidth variation, and Fig. 7(a) and (b) shows the corresponding values of r and θ_0 required to

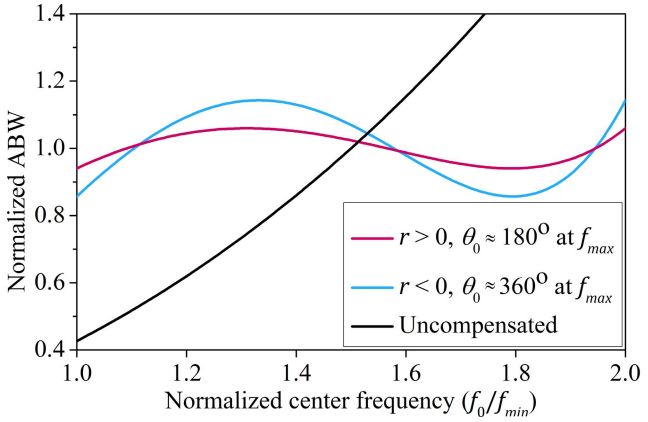

Fig. 7. Coupling ratio r and transmission line length θ_0 required for constant bandwidth, plotted versus tuning range for (a) $r < 0$ and (b) $r > 0$.

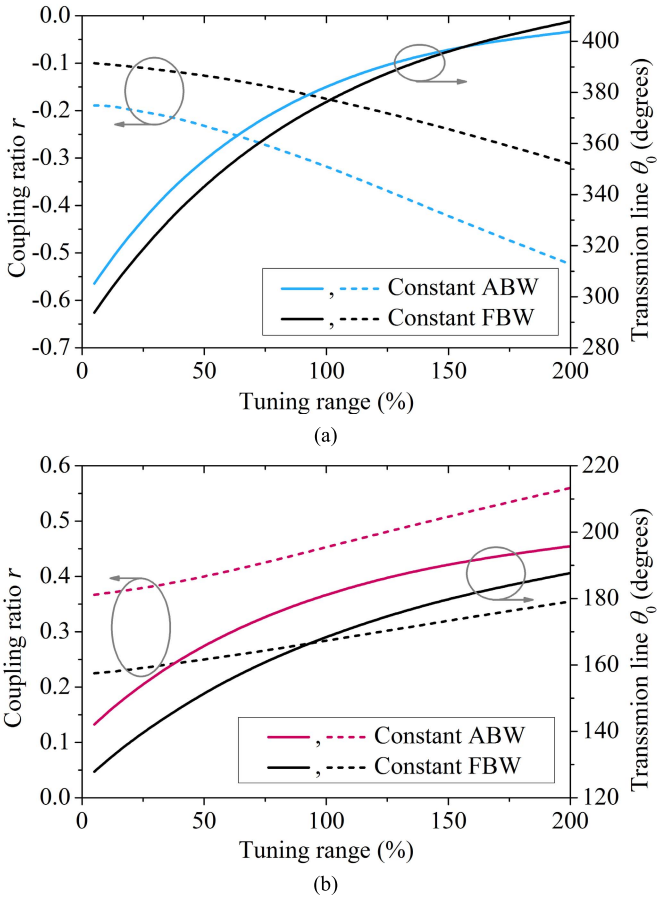

Fig. 8. Frequency variation of ABW for $r > 0$ and $r < 0$. Because a longer transmission line is required, the bandwidth compensation method is less effective when $r < 0$, resulting in roughly twice as much bandwidth variation.

minimize bandwidth variation. For example, over an octave (100%) tuning range, the proposed method can reduce the FBW variation from 125% to just 3.5% (a 97% reduction), and can reduce the ABW variation from 350% to just 12% (a 96.5% reduction). Reducing the tuning range to 50% greatly reduces the amount of bandwidth variation. In this case the FBW variation can be reduced from 56% to approximately 0.7% (a 99% reduction), and the ABW variation can be reduced from 130% to approximately 2% (a 98.5% reduction). Fig. 7 also shows the difference between utilizing coupling elements of the same sign ($r > 0$), which requires a transmission line which is about 180° at $f_{\max}$, and utilizing coupling elements of opposite sign ($r < 0$), which requires a transmission line which is approximately 360° at $f_{\max}$. It is evident that significantly less bandwidth variation can be obtained when coupling elements of the same sign are used. This is because compared to a nominally 360° transmission line, the nominally 180° transmission line experiences half as much variation in phase over a given tuning range, and the shaping factor F is therefore more linear for the given frequency range and more effective at compensating the frequency dependence of the coupling element. Because of this it is always desired, if possible, to use coupling elements of the same sign so that a nominally 180° transmission line can be used. This might not always be possible, however, especially at high frequencies or when using high-permittivity substrates (see [15], [16]) which could make it impossible to physically realize a transmission line which is less than 180° between the coupling elements. Fig. 8 shows the frequency dependence of the total coupling coefficient when a 360° transmission line is used ($r < 0$) compared to when a 180° transmission line is used ($r > 0$).

B. Phase Variation

A two-pole absorptive bandstop filter (see [17]) implemented using the coupling topology of Fig. 1(a) has the structure shown in Fig. 9(a). The length of transmission line between the two resonators does not have a significant effect on the bandwidth of the filter, but it does affect the symmetry of the filter's transfer function. In order to have a symmetric transfer function, a transmission line of length

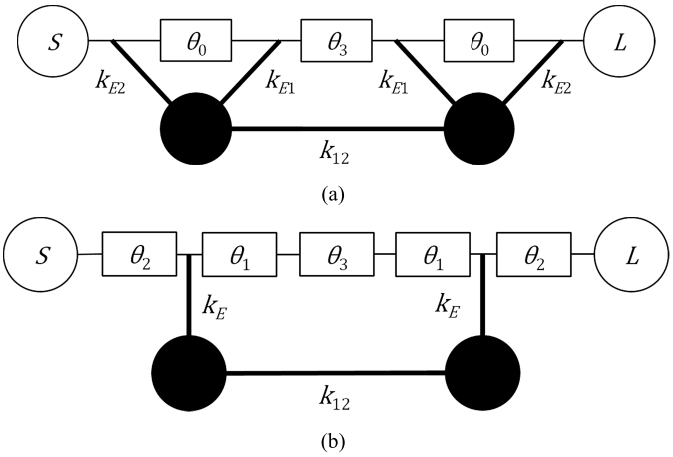

Fig. 9. (a) Topology of a two-pole bandstop filter using the constant-coupling structure of Fig. 1(a). (b) Topology from (a) using equivalent circuit for the coupling structure from Fig. 1(b).

θ_3 must be inserted in order to provide 90° phase between the resonators [18]. Replacing the twice-coupled resonators in Fig. 9(a) with their equivalent circuits [Fig. 1(b)] yields the circuit of Fig. 9(b), showing that the phase contributed by the constant-coupling structure must be taken into account when

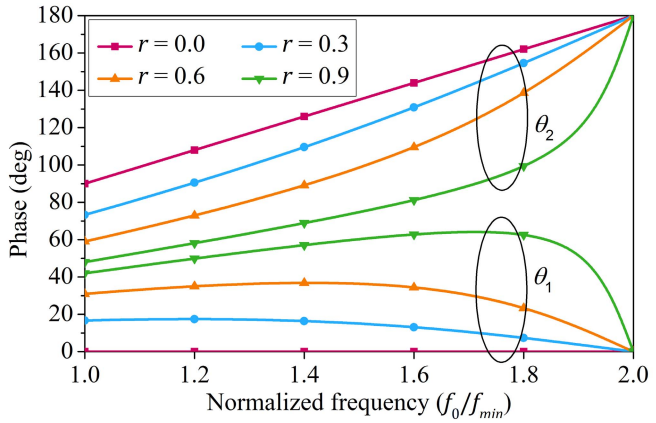

Fig. 10. Frequency variation of phase lengths θ_1 and θ_2 for different values of r. $\theta_0 = 180°$ at $f_{\max}$.

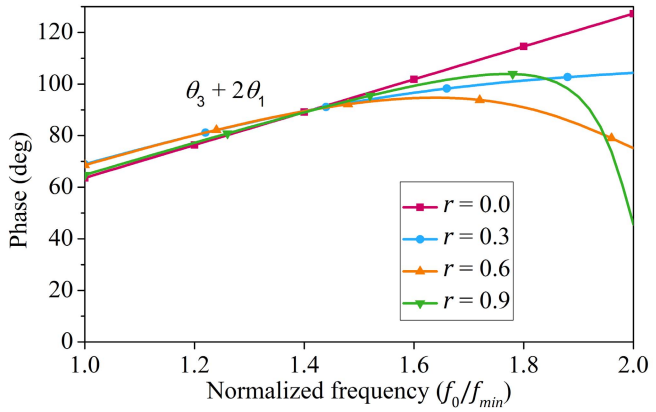

Fig. 11. Frequency variation of total phase between resonators, equal to θ_3 (the physical transmission line added between the resonators) $+2\theta_1$ (the phase contributed by the coupling structure).

selecting the length of transmission line θ_3. If (5) is substituted into (3), the equation for θ_1 can be reformulated as

$$\theta_1 = \frac{1}{2}\left(\pi - \arg\left(-\frac{r + e^{-j\theta_0}}{r + e^{j\theta_0}}\right)\right) \tag{12}$$

while (4) remains the same. We see that the equivalent lengths of transmission line which define the coupling reference plane depend not only on the length of transmission line in the coupling section, but also on the ratio of the two coupling values. If we examine the frequency variation of θ_1 and θ_2 for different values of r (plotted in Fig. 10), we can see that θ_2 increases monotonically with frequency. θ_1 is not monotonic, however, and actually has a negative slope versus frequency for some frequencies.

This negative phase-versus-frequency slope can be beneficial, as it reduces the frequency variation of the phaselength between the two resonators. The total phase between the resonators is equal to the sum of the physical transmission line length θ_3 and twice the virtual phaselength θ_1. It has less phase variation over a given tuning range than a single length of TEM transmission line would because of the negative frequency dependence of θ_3. This is shown in Fig. 11. It can be seen that for a coupling ratio of $r = 0$, which is the case of only a single coupling aperture, the total phase between the resonators changes by 100% over an octave tuning range (63.6°–127.3°) as expected because $\theta_1 = 0$ and all of the phase between the resonators is provided by the TEM transmission line θ_3. As r is increased, the variation in phase decreases, and can be as little as 38% (68.5°–94.7° for $r = 0.6$). This reduction in phase variation helps the filter to maintain a symmetric transfer function when tuned over a wide frequency range.

Because the phase between the resonators does not strongly affect the filter's bandwidth, (12) is generally not taken into account when optimizing the coupling coefficients for constant bandwidth. However, it does provide useful information when choosing the length of transmission line between the resonators for a symmetric transfer function.

III. Constant-Bandwidth Filter Design

Tunable evanescent-mode cavity resonators were chosen as the technology for the filters in this paper due to their well-known high unloaded quality factors and wide tuning ranges.

This kind of resonator consists of a substrate-integrated waveguide cavity loaded with a capacitive post which is connected to the bottom of the cavity. A small gap is left between the post and the top of the cavity, which approximates a parallel-plate capacitor and gives a method for tuning the frequency of the resonator if the ceiling of the cavity can be displaced by an actuator, such as a piezoelectric disc [19] or an electrostatically actuated MEMS diaphragm [20]. The features and design of these resonators will not be further discussed here because of the abundance of information available in open literature [21]–[23].

Five filters were designed in order to validate the concepts described in Section II. Filter A is a 1.2% constant-FBW filter with a 3–6-GHz tuning range. Filter B is a 53-MHz constant-ABW filter with a 3–6-GHz tuning range. Filter C is a 53-MHz constant-ABW filter with a 3.5–5.5-GHz tuning range in order to demonstrate the tradeoff between bandwidth variation and tuning range. Filter D is a four-pole constant-ABW filter consisting of a back-to-back cascade of two Filter B's. Filter E is an uncompensated filter which does not use the presented constant-bandwidth coupling method, but instead uses a single coupling element. This filter allows for a fair evaluation of the performance gained by using the constant-bandwidth coupling structure.

To increase the filters' stopband rejection, an absorptive bandstop filter design is used [17]. By choosing $k_E \geq (2/Q_U)^{1/2}$, and $k_{12} \approx 1/Q_U$, where Q_U is the unloaded quality factor of the constituent resonators, the filter can achieve theoretically infinite stopband attenuation even with finite-Q_U resonators. It should be noted that k_{12} is much smaller than k_E, and as a result has little impact on the filter's bandwidth and does not fundamentally change the analysis of Section II.

When cascading two-pole filter sections in order to create a four-pole filter, as in the case of Filter D, a 90° transmission line should be inserted between stages in order to provide the impedance matching required for a symmetric transfer function. This phaselength should take into account the

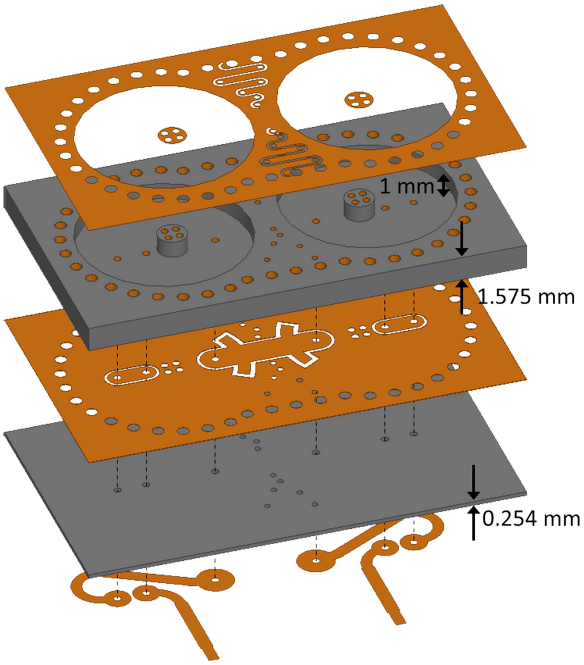

Fig. 12. Exploded view of the designed two-pole constant-bandwidth filters.

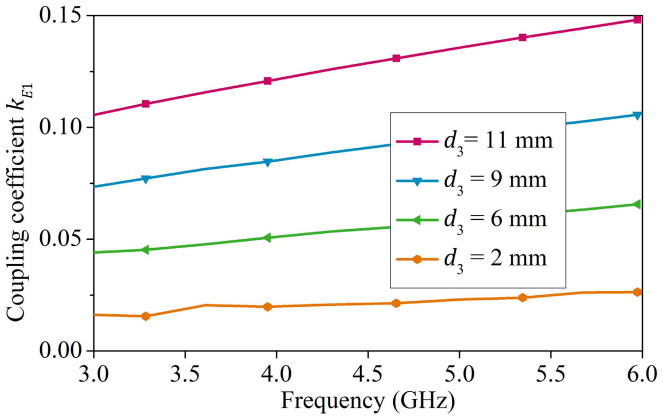

Fig. 13. Frequency variation of the coupling coefficient k_{E1} for various lengths of d_3. In these simulations, $w_2 = 2$ mm and $\phi = 0$.

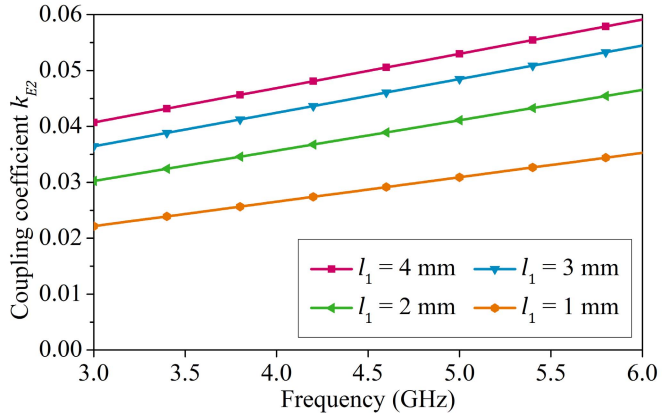

Fig. 14. Frequency variation of k_{E2} for various lengths of l_1. $w_1 = 1$ mm in these simulations.

phaselength θ_2 contributed by the constant-bandwidth coupling structure, as shown in Fig. 9. However, the designed filters are partially absorptive at their center frequencies, and there is little impedance mismatch between sections. As a result, the inter-stage transmission line length is not critical, and the two-pole stages can simply be placed as close together as possible.

A. External Coupling

The filters proposed in our paper use a coupling structure in which the microstrip feeding line is transferred to a coplanar waveguide (CPW) transmission line embedded in the ground plane, which is shared with the cavity. This structure is shown in Figs. 12 and 15(a) and (b). The magnetic field of this section of CPW couples with the magnetic field of the cavity, realizing the desired external coupling. The strength of the coupling depends on both the length and width of the section of CPW line embedded in the cavity's ground plane. To increase the coupling coefficient, radially oriented stubs can also be added to this section of CPW line in order to increase the area of the CPW section inside the cavity. The coupling coefficient k_{E1} is determined by the CPW length and width d_3 and w_2, as well as the radial stub angle ϕ. The value of k_{E2} is determined by the CPW length and width l_1 and w_1. The values of k_{E1} and k_{E2} can be extracted from electromagnetic simulation using the method in [24], or by calculating the external quality factor Q_E with the method in [25] and using the relationship $k_{E1,2} = \sqrt{2/Q_{E1,2}}$. Fig. 13 shows the frequency dependence of the coupling coefficient k_{E1} produced by this coupling structure for various lengths of d_3, and Fig. 14 shows the simulated values of k_{E2} for various lengths of l_1. It can be seen that the coupling coefficients are approximately linear with respect to frequency and increase by about 50% over an octave tuning range, which justifies the model used for the coupling coefficients used in Section II.

B. Polarity of External Coupling Structures

As can be seen from Fig. 2, the relative sign of the external coupling elements must be known in order to design a constant-bandwidth coupling structure.

If a cavity using the coupling structure just described is excited with a signal from the left side of the structure with the excitation de-embedded such that the reference plane is in the middle of the coupling section, the magnetic field in the cavity aligns with the magnetic field of the transmission line and is oriented in a counterclockwise direction, as shown in Fig. 15(a). However, if the coupling section is placed on the opposite side of the cavity and the same excitation is applied, again de-embedding the reference plane to the center of the coupling element, the magnetic field in the cavity has the opposite orientation, as seen in Fig. 15(b). From this we see that two coupling structures with exactly the same size and shape can yield opposite sign of coupling depending on the direction of signal propagation across the coupling section with respect to the orientation of the cavity.

Since it is desirable for the two coupling elements to have the same polarity (see Section II-A), the coupling sections

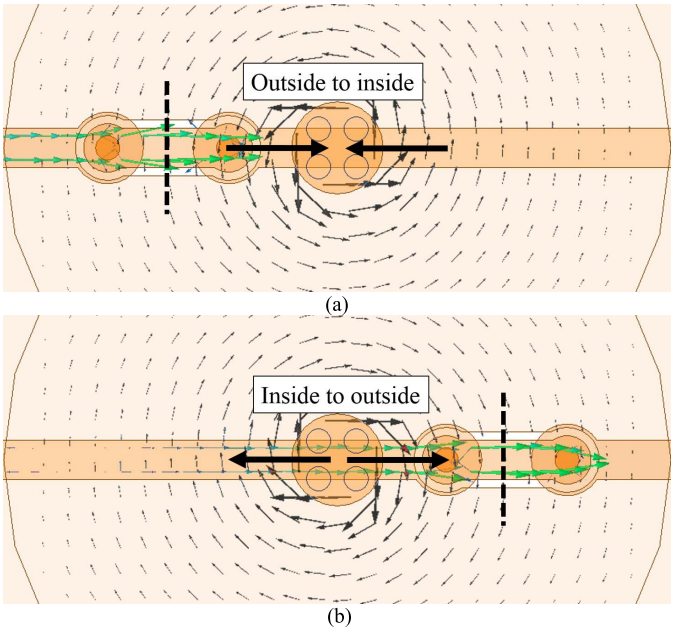

Fig. 15. Current density on the microstrip line (green arrows) and magnetic field inside the cavity (black arrows) when the incident signal propagates. (a) From the outside of the cavity to the inside. (b) From the inside of the cavity to the outside. The thick arrows indicate the inside and the outside of the cavity, and the dashed lines indicate the simulation reference planes. Because the magnetic field has the opposite direction in the two cases, the sign of the coupling for the two cases is opposite.

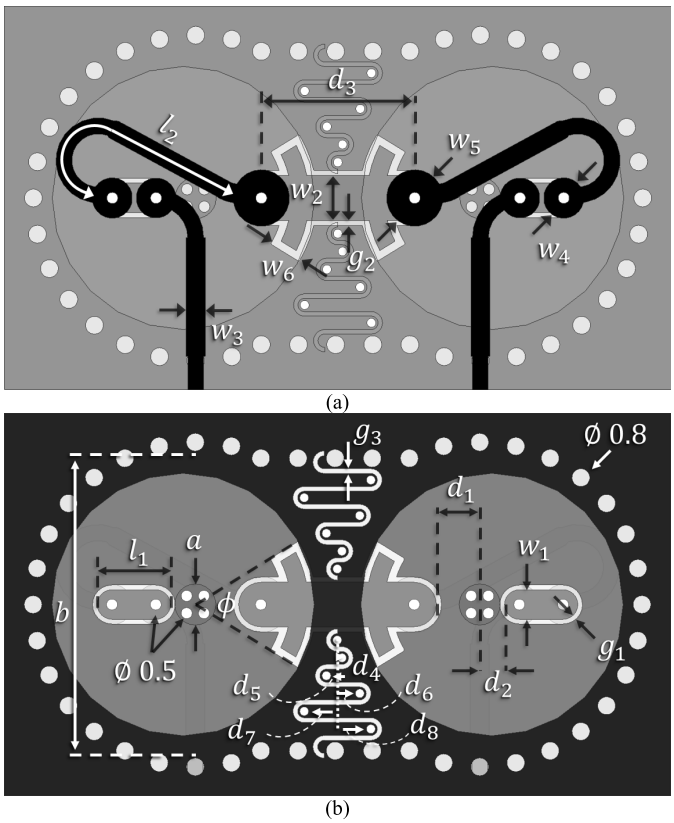

Fig. 16. Layout of filters A, B, and C. Dimensions are shown as follows (in millimeters) and in Table I. $a = 1.9$, $b = 13.8$, $d_4 = 0.2$, $d_5 = 0.5$, $d_6 = 1$, $d_7 = 1.5$, $d_8 = 1.5$, $g_3 = 0.15$, $w_3 = 0.86$.

must be oriented such that the direction of signal propagation across each element is the same: either from inside of the cavity to outside the cavity, or outside the cavity to the inside. To accomplish this, the transmission line between the coupling elements is looped around the smaller coupling section, so that for both coupling elements a signal launched from the input will propagate from the inside of the cavity to the outside.

With the knowledge of the frequency-dependent coupling values k_{E1} and k_{E2}, (2) was used to optimize the ratio between the coupling values and the length of transmission line between them in order to minimize the frequency variation in coupling coefficient for Filter A, and ABW for Filters B–D.

C. Inter-Resonator Coupling

Inter-resonator coupling between evanescent-mode cavity resonators is typically realized by a coupling iris consisting of a below-cutoff section of substrate-integrated waveguide. When this is used to realize an absorptive bandstop filter, a transmission line which is nominally 270° at the midpoint of the filter's tuning range is required between the resonators in order to achieve destructive signal interference and provide very high levels of stopband attenuation [26], [27]. It would be preferable to instead use a length of transmission line which is nominally 90°, as this would yield a wider tuning range over which the filter could achieve high stopband rejection, because the required phase relationship between the inter-resonator coupling and the transmission line would be upheld over a wider tuning range. This requires the inter-resonator coupling to take on the opposite sign.

The method used in this filter is derived from the methods for reversing the sign of inter-resonator coupling presented in [28] and [29]. An array of vias is used to connect the top and bottom conductors of the coupling iris section together, and a slot is cut into the copper of the upper conducting layer. This slot blocks the current flowing on the top conductor, and reroutes it onto the bottom conductor through the vias. This effectively reverses the direction of the current in the coupling section, which in turn yields a coupling value which is opposite compared to that of the original coupling iris. The inter-resonator coupling dimensions, such as the spacing between the vias and the width of the coupling iris, were determined through full-wave electromagnetic simulations in order to yield the coupling required for the absorptive bandstop filter ($k_{12} \approx 1/Q_U$). The simulated quality factor of the resonators was approximately 400 at the center of the tuning range, and thus k_{12} was designed to be approximately 0.0025. The final dimensions of the filters are listed in Fig. 16 and Table I. Filter D consists of two copies of Filter B cascaded back to back as shown in Fig. 17, and thus its dimensions are not shown in Table I. The layout of Filter E is shown in Fig. 18. Additional information about Filter E can be found in [30].

IV. Fabrication and Measurements

The filters were fabricated using a commercially available PCB milling, laminating, and plating system. The signal and cavity substrates were made out of 0.25- and 1.58-mm-thick

TABLE I
SUMMARY OF DIMENSIONS OF THE DESIGNED FILTERS IN MILLIMETERS

Filter	d_1	d_2	d_3	g_1	g_2	l_1	l_2	φ	w_1	w_2	w_4	w_5	w_6
A	0.71	2.0	10.2	0.21	0.24	2.35	14.0	0^o	1.0	1.9	1.4	2.0	---
B	1.8	1.11	6.9	0.19	0.23	3.3	13.7	63^o	1.33	2.2	1.83	2.61	1.5
C	1.8	1.29	7.0	0.19	0.23	3.13	14.3	63^o	1.33	2.2	1.83	2.61	1.5
E	1.0	---	10.1	---	0.26	---	---	0^o	---	1.9	---	1.9	---

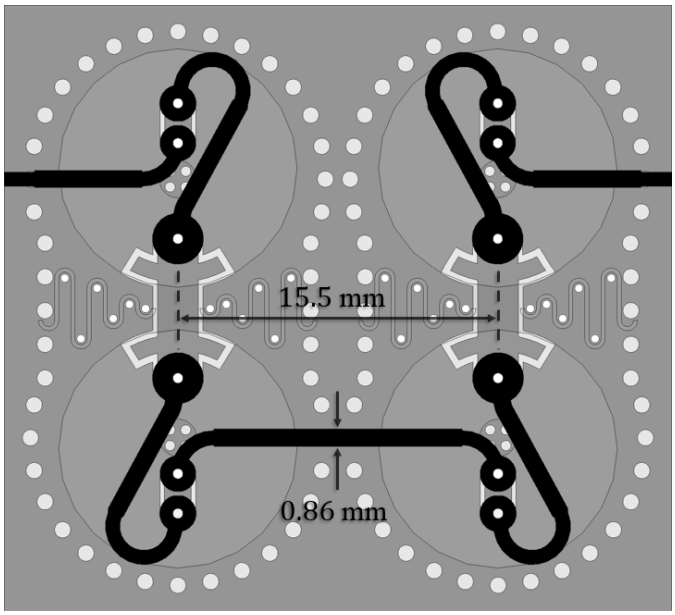

Fig. 17. Layout of Filter D, comprising two cascaded Filter B's.

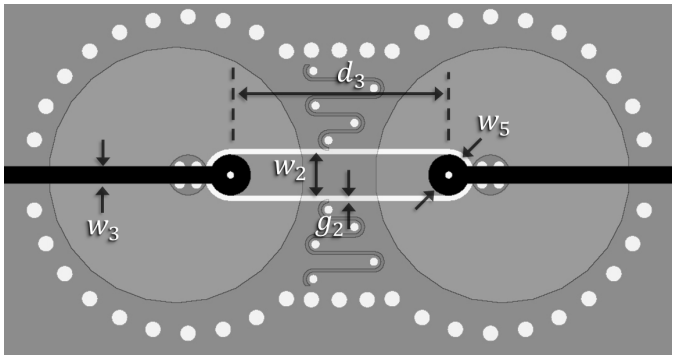

Fig. 18. Layout of uncompensated filter (filter E). Except for a few minor differences in dimensions (as noted in Table I), it is identical to Filter A with the smaller coupling element removed.

Rogers 5880, respectively, and were laminated together using Rogers 2929 bondply material. Piezoelectric discs (Piezo Systems T216-A4NO-273X) were used as the tuning elements. The discs were metalized with thin silver membranes and attached on top of the cavities using electrically conductive epoxy, and were actuated by applying a −200- to +200-V bias voltage to the tops of the discs using dc probes. Because the top electrodes of the piezoelectric discs are electrically isolated from the resonator cavities, no special biasing circuitry

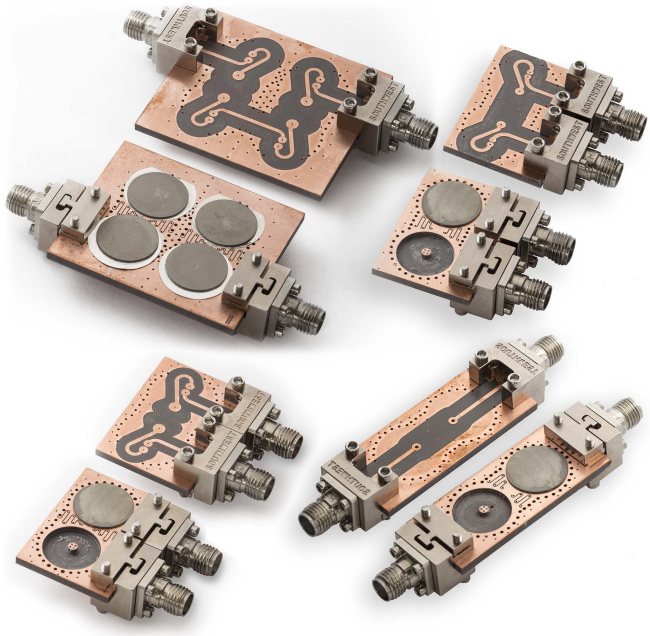

Fig. 19. Photograph of the fabricated filters. The top and bottom of each filter are shown. Clockwise, from top left: Filter D, Filter A, Filter E, Filter B. Filter C is not shown because it is nearly visually indistinguishable from Filter B.

is required. A photograph of the top and bottom sides of the filters is shown in Fig. 19, with the piezoelectric tuning discs removed from some of the resonators in order to show the insides of the cavities.

A. Constant-FBW Filter

Fig. 20 shows the measured response of Filter A when tuned to 4.8 GHz. The filter has over 70 dB of stopband rejection due to the absorptive filter design, and the passband is low-loss and well-matched, with better than 15 dB of passband return loss and less than 0.5 dB of insertion loss up to 7 GHz. The performance of Filter A when tuned across its octave tuning range is shown in Fig. 21. It tunes from 3.2 to 6.4 GHz, maintaining over 60 dB of stopband rejection for all tuning states.

In order to investigate the relative improvement gained by the constant-bandwidth coupling method, the 3- and 10-dB bandwidths of both the uncompensated filter (Filter E) and the constant-FBW filter (Filter A) were measured across their tuning ranges, and are shown in Fig. 22. Filter E's 3- and 10-dB bandwidths vary from 1.25% to 2.3%

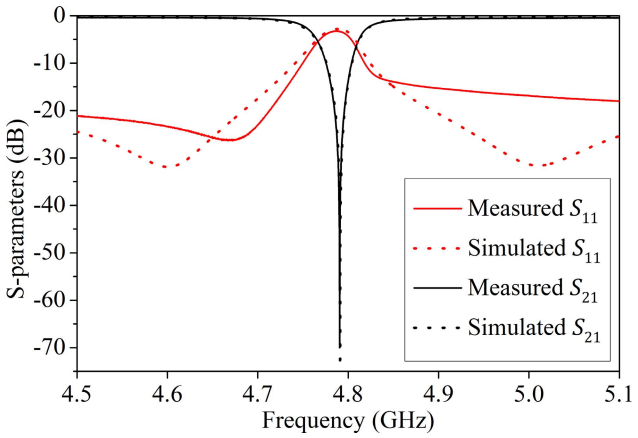

Fig. 20. Measured response of Filter A when tuned to 4.8 GHz.

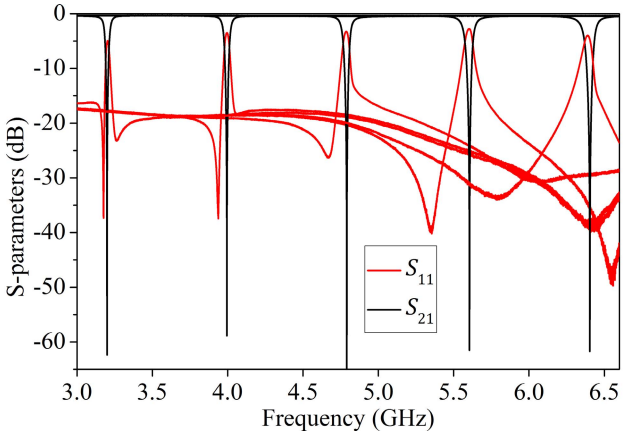

Fig. 21. S-parameters of Filter A across its octave tuning range.

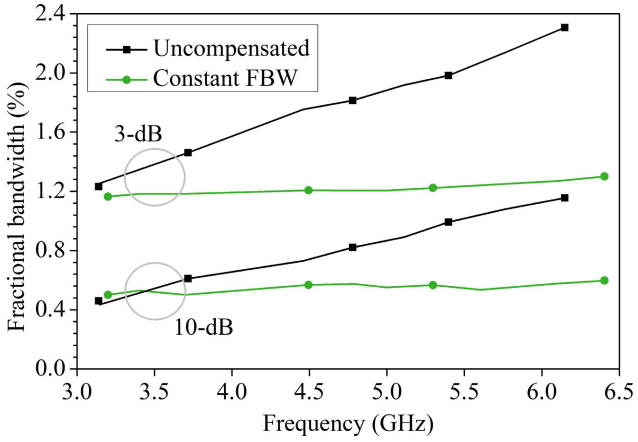

Fig. 22. Measured 3- and 10-dB FBWs of Filter A, compared to that of the uncompensated filter E.

(84% variation) and 0.43%–1.16% (170% variation), respectively. The constant-FBW filter has greatly reduced bandwidth variation, with a 1.16%–1.3% 3-dB bandwidth (12% variation) and a 0.5%–0.6% 10-dB bandwidth (20% variation). Compared to Filter E, Filter A has an 86% reduction in 3-dB FBW variation and an 88% reduction in 10-dB FBW variation.

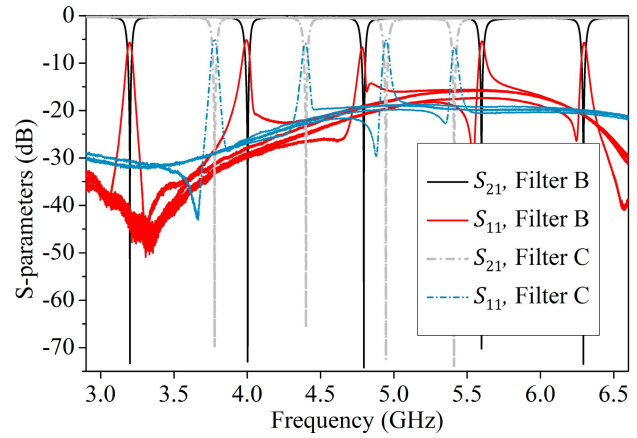

Fig. 23. Measured S-parameters of filters B and C (constant-ABW filters with 100% and 50% tuning ranges, respectively).

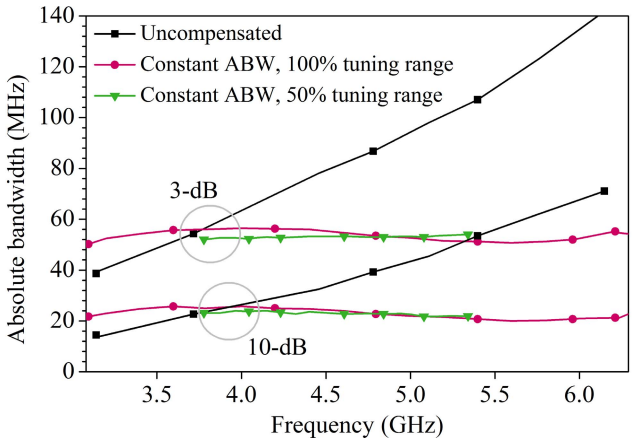

Fig. 24. Measured 3- and 10-dB bandwidths of filters B and C (constant-ABW filters with 100% and 50% tuning ranges) and the uncompensated filter E.

B. Constant-ABW Filters

The two filters optimized for constant ABW, one over a 100% tuning range (Filter B) and the other over a 50% tuning range (Filter C), were measured. Their S-parameters are plotted in Fig. 23. The measured ABW of both filters, along with that of Filter E, are shown in Fig. 24. The 3- and 10-dB bandwidths of the uncompensated filter E are 39–142 MHz (a 264% variation) and 14.4–71 MHz (393% variation), respectively. The filter optimized for constant ABW over a 100% tuning range (Filter B) experiences much less bandwidth variation, and has a 50.3–56.5-MHz 3-dB bandwidth (12.3% variation), and a 20–25.8-MHz 10-dB bandwidth (29% variation). Compared to the uncompensated filter, Filter B realizes a 95% reduction in 3-dB bandwidth variation, and a 93% reduction in 10-dB bandwidth variation.

The filter optimized for a 50% tuning range experiences even less bandwidth variation, and has a 52–54-MHz 3-dB bandwidth (3.8% variation), and a 21.8–24-MHz 10-dB bandwidth (10% variation).

Note that because the unloaded quality factors of the resonators change across the filter's tuning range, it is impossible

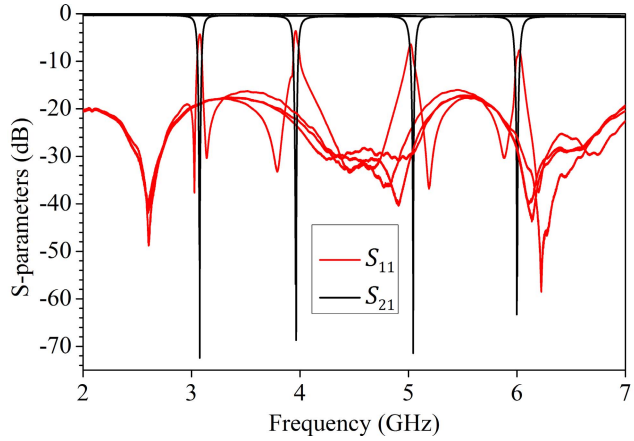

Fig. 25. Measured S-parameters of four-pole constant-ABW filter with notches synchronously tuned for maximum stopband attenuation.

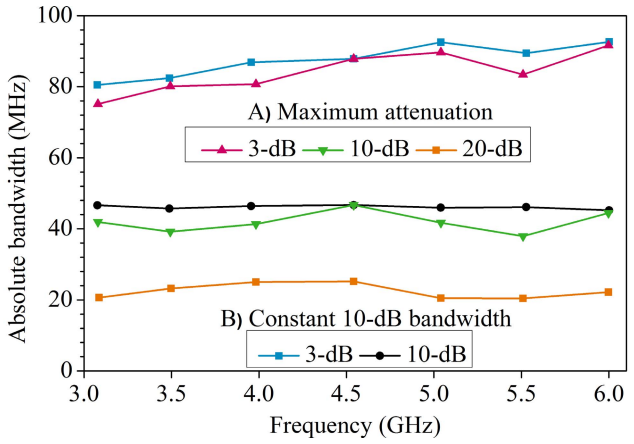

Fig. 26. Measured bandwidth versus center frequency for the four-pole filter in two states: A) both notches are synchronously tuned in order to provide maximum attenuation and B) notches are asynchronously tuned in order to maintain a constant 10-dB bandwidth.

to simultaneously minimize the 3- and 10-dB bandwidths. In these designs, the filters were optimized for constant 3-dB bandwidth, but the filters could be similarly optimized for minimum 10-dB bandwidth variation.

C. Four-Pole Filter

The four-pole constant-ABW filter was measured with the notches of each stage synchronously tuned in order to provide maximum attenuation, as shown in Fig. 25. The 3-, 10-, and 20-dB bandwidths were measured and are plotted in Fig. 26. It maintains a fairly constant 75.2–91.7-MHz 3-dB bandwidth across its octave tuning range.

The four-pole filter offers an additional degree of freedom in reconfigurability compared to the two-pole filters, since it consists of two cascaded absorptive notch sections which can be either synchronously or asynchronously tuned. This allows the filter to produce a variety of transfer functions, as shown in Fig. 27. Synchronously tuning the notches provides maximum attenuation, and asynchronously tuning the notches provides a Chebyshev-like frequency response. Asynchronously tuning the notches also allows the bandwidth

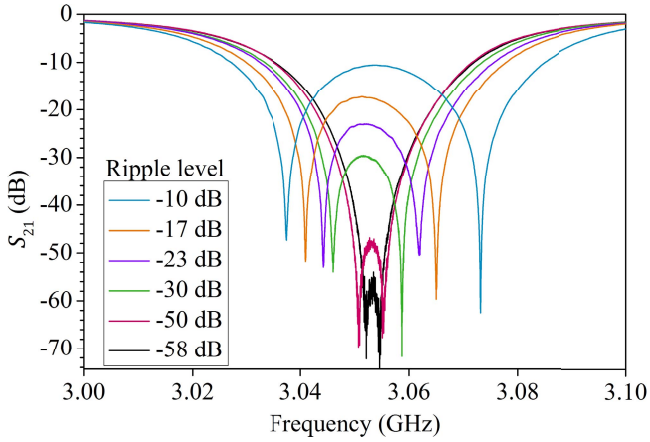

Fig. 27. Measured response of four-pole filter when tuned to different levels of stopband ripple and increased bandwidth.

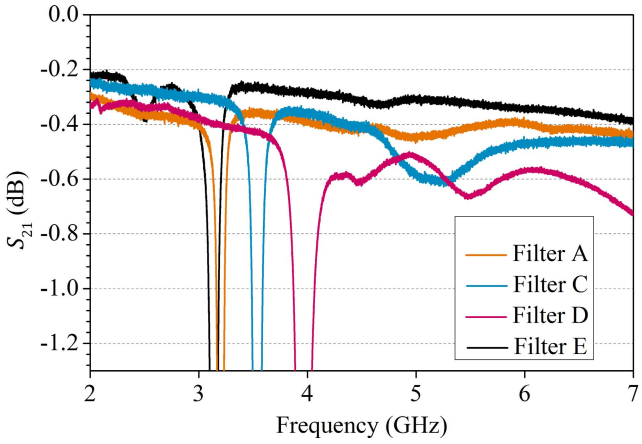

Fig. 28. Comparison of the passband loss of the filters.

of the filter be tuned slightly, and it is possible to use this bandwidth tunability to compensate for any residual bandwidth variation. Using this method, the filter was again tuned from 3 to 6 GHz, while asynchronously tuning the notches in order to maintain a constant 46-MHz 10-dB bandwidth. The 10-dB bandwidth is maintained nearly perfectly constant, and is only limited by the accuracy with which the two notches are tuned. The 3- and 10-dB bandwidths are shown in Fig. 26. There was approximately 1.5 MHz of bandwidth variation in these measurements, but this could be reduced further by more accurately tuning the notches. In order to maintain constant 10-dB bandwidth, the stopband ripple varied from a minimum of −55 dB at 4 GHz to a maximum of −15 dB at 5.5 GHz.

D. Insertion Loss of Filters

Because the constant bandwidth coupling method requires additional lengths of transmission lines, it also has slightly higher passband insertion loss compared to the uncompensated design. A close-up view of the passbands of all the filters is shown in Fig. 28. The uncompensated filter has 0.3 dB of insertion loss at 6 GHz, which as expected is lower than all of the other filters. Filters A and C have approximately 0.1 dB more insertion loss than Filter E at 6 GHz, and Filter D has roughly 0.2 dB more insertion loss than Filters A and C.

TABLE II
COMPARISON OF OUR WORK TO EXISTING STATE-OF-THE-ART CONSTANT-ABSOLUTE-BANDWIDTH TUNABLE BANDSTOP FILTERS

Ref.	Technology	Tuning Range	Maximum Frequency	ABW Variation
[8]	Lumped	175%	55 MHz	~20%*
[9]	Lumped	142%	135 MHz	~40%*
[10]	Microstrip	93%	930 MHz	24%*
[11]	Microstrip	27%	2.2 GHz	12.8%†
Filter B	3-D cavity	100%	6.3 GHz	12.3%*
Filter C	3-D cavity	50%	5.4 GHz	3.8%*
Filter D	3-D cavity	96%	6.0 GHz	3.2%††

* 3-dB bandwidth † 20-dB bandwidth †† 10-dB bandwidth

E. Comparison to State of the Art

In order to evaluate the relative effectiveness of this method of achieving constant bandwidth, Table II compares the results of the filters in this paper to other constant-bandwidth tunable bandstop filters. It can be seen that the method presented in this paper achieves significantly less bandwidth variation for a given tuning range than the two examples which use microstrip resonators [10], [11]. Its bandwidth variation performance is also better than [9], and is comparable to [8]. Since [8] and [9] are implemented with lumped elements, however, it is clear that the method presented in this paper has state-of-the-art performance for frequencies higher than those permitted by lumped-element filters.

V. CONCLUSION

In this paper, a new coupling method which was recently introduced in [14] was investigated in greater detail. It is shown that the coupling method can partially compensate for the frequency dependence inherent to practical coupling structures, yielding a coupling coefficient which either is nearly constant as required for constant FBW, or decreases with respect to frequency in order to have constant ABW. Several design tradeoffs are investigated, and it is shown that less bandwidth variation can be obtained for narrower tuning ranges than for larger tuning ranges. To validate the theory and design principles, several filters were designed, fabricated, and measured: a constant-FBW filter with a 1.16%–1.3% 3-dB bandwidth; a constant-ABW filter with an octave tuning range and a 53.4 ± 3.1-MHz 3-dB bandwidth; a constant-ABW with a 50% tuning range and a 53 ± 1-MHz 3-dB bandwidth; and a constant-ABW four-pole filter which can maintain a constant 46-MHz 10-dB bandwidth. These results are compared to other published constant-bandwidth bandstop filters, and it is shown that the method presented in this paper is the most effective method for reducing bandwidth variation at frequencies where lumped-element resonators cannot be used.

REFERENCES

[1] E. J. Naglich, J. Lee, D. Peroulis, and W. J. Chappell, "Bandpass–bandstop filter cascade performance over wide frequency tuning ranges," *IEEE Trans. Microw. Theory Techn.*, vol. 58, no. 12, pp. 3945–3953, Dec. 2010.

[2] T.-C. Lee, J. Lee, and D. Peroulis, "Dynamic bandpass filter shape and interference cancellation control utilizing bandpass–bandstop filter cascade," *IEEE Trans. Microw. Theory Techn.*, vol. 63, no. 8, pp. 2526–2539, Aug. 2015.

[3] E. J. Naglich, J. Lee, and D. Peroulis, "Tunable bandstop filter with a 17-to-1 upper passband," in *IEEE MTT-S Int. Microw. Symp. Dig.*, Jun. 2012, pp. 1–3.

[4] K. W. Wong, R. R. Mansour, and G. Weale, "Compact tunable bandstop filter with wideband balun using IPD technology for frequency agile applications," in *IEEE MTT-S Int. Microw. Symp. Dig.*, May 2015, pp. 1–3.

[5] I. Reines, S.-J. Park, and G. M. Rebeiz, "Compact low-loss tunable *X*-band bandstop filter with miniature RF-MEMS switches," *IEEE Trans. Microw. Theory Techn.*, vol. 58, no. 7, pp. 1887–1895, Jul. 2010.

[6] A. Anand, Y. Liu, and X. Liu, "Substrate-integrated octave-tunable combline bandstop filter with surface mount varactors," in *Proc. IEEE Int. Wireless Symp. (IWS)*, Mar. 2014, pp. 1–4.

[7] A. C. Guyette, "Intrinsically switched varactor-tuned filters and filter banks," *IEEE Trans. Microw. Theory Techn.*, vol. 60, no. 4, pp. 1044–1056, Apr. 2012.

[8] D. R. Jachowski, "Octave tunable lumped-element notch filter," in *IEEE MTT-S Int. Microw. Symp. Dig.*, Jun. 2012, pp. 1–3.

[9] T.-C. Lee, J. Lee, E. J. Naglich, and D. Peroulis, "Octave tunable lumped-element notch filter with resonator-Q-independent zero reflection coefficient," in *IEEE MTT-S Int. Microw. Symp. Dig.*, Jun. 2014, pp. 1–4.

[10] D. R. Jachowski and A. C. Guyette, "Sub-octave-tunable microstrip notch filter," in *Proc. IEEE Int. Symp. Electromagn. Compat.*, Aug. 2009, pp. 99–102.

[11] X. Y. Zhang, C. H. Chan, Q. Xue, and B. J. Hu, "RF tunable bandstop filters with constant bandwidth based on a doublet configuration," *IEEE Trans. Ind. Electron.*, vol. 59, no. 2, pp. 1257–1265, Feb. 2012.

[12] A. C. Guyette, "Varactor-tuned bandstop filters with tunable center frequency and bandwidth," in *Proc. IEEE Int. Conf. Wireless Inf. Technol. Syst. (ICWITS)*, Aug./Sep. 2010, pp. 1–4.

[13] A. Anand and X. Liu, "Capacitively tuned electrical coupling for reconfigurable coaxial cavity bandstop filters," in *IEEE MTT-S Int. Microw. Symp. Dig.*, May 2015, pp. 1–3.

[14] M. D. Hickle and D. Peroulis, "Octave-tunable constant absolute bandwidth bandstop filter utilizing a novel passively-compensated coupling method," in *IEEE MTT-S Int. Microw. Symp. Dig.*, May 2016, pp. 1–3.

[15] M. D. Hickle, M. D. Sinanis, and D. Peroulis, "Design and implementation of an intrinsically-switched 22–43 GHz tunable bandstop filter," in *Proc. IEEE 17th Annu. Wireless Microw. Technol. Conf. (WAMICON)*, Apr. 2016, pp. 1–4.

[16] M. D. Hickle, M. D. Sinanis, and D. Peroulis, "Tunable high-isolation W-band bandstop filters," in *IEEE MTT-S Int. Microw. Symp. Dig.*, May 2015, pp. 1–3.

[17] D. R. Jachowski, "Compact, frequency-agile, absorptive bandstop filters," in *IEEE MTT-S Int. Microw. Symp. Dig.*, Jun. 2005, pp. 1–4.

[18] A. C. Guyette and E. J. Naglich, "Short-through-line bandstop filters using dual-coupled resonators," *IEEE Trans. Microw. Theory Techn.*, vol. 64, no. 2, pp. 459–466, Feb. 2016.

[19] H. Joshi, H. H. Sigmarsson, D. Peroulis, and W. J. Chappell, "Highly loaded evanescent cavities for widely tunable high-Q filters," in *IEEE MTT-S Int. Microw. Symp. Dig.*, Jun. 2007, pp. 2133–2136.

[20] X. Liu, L. P. B. Katehi, W. J. Chappell, and D. Peroulis, "A 3.4–6.2 GHz continuously tunable electrostatic MEMS resonator with quality factor of 460–530," in *IEEE MTT-S Int. Microw. Symp. Dig.*, Jun. 2009, pp. 1149–1152.

[21] H. Joshi, H. H. Sigmarsson, S. Moon, D. Peroulis, and W. J. Chappell, "High-*Q* fully reconfigurable tunable bandpass filters," *IEEE Trans. Microw. Theory Techn.*, vol. 57, no. 12, pp. 3525–3533, Dec. 2009.

[22] X. Liu, L. P. B. Katehi, W. J. Chappell, and D. Peroulis, "High-*Q* tunable microwave cavity resonators and filters using SOI-based RF MEMS tuners," *J. Microelectromech. Syst.*, vol. 19, no. 4, pp. 774–784, Aug. 2010.

[23] D. Peroulis, E. Naglich, M. Sinani, and M. Hickle, "Tuned to resonance: Transfer-function-adaptive filters in evanescent-mode cavity-resonator technology," *IEEE Microw. Mag.*, vol. 15, no. 5, pp. 55–69, Jul./Aug. 2014.

[24] M. D. Hickle, "Synthesis, design, and fabrication techniques for reconfigurable microwave and millimeter-wave filters," Ph.D. dissertation, School Elect. Comput. Eng., Purdue Univ., West Lafayette, IN, USA, 2016, pp. 155–161.

[25] D. Kajfez and P. Guillon, Eds., *Dielectric Resonators*. Atlanta, GA, USA: Noble, 1998, pp. 474–480.

[26] T. Snow, J. Lee, and W. J. Chappell, "Tunable high quality-factor absorptive bandstop filter design," in *IEEE MTT-S Int. Microw. Symp. Dig.*, Jun. 2012, pp. 1–3.
[27] E. J. Naglich, A. C. Guyette, and D. Peroulis, "High-Q intrinsically-switched quasi-absorptive tunable bandstop filter with electrically-short resonators," in *IEEE MTT-S Int. Microw. Symp. Dig.*, Jun. 2014, pp. 1–4.
[28] E. J. Naglich, D. Peroulis, and W. J. Chappell, "Wide spurious free range positive-to-negative inter-resonator coupling structure for reconfigurable filters," in *IEEE MTT-S Int. Microw. Symp. Dig.*, Jun. 2013, pp. 1–4.
[29] X.-P. Chen and K. Wu, "Substrate integrated waveguide cross-coupled filter with negative coupling structure," *IEEE Trans. Microw. Theory Techn.*, vol. 56, no. 1, pp. 142–149, Jan. 2008.
[30] M. D. Hickle and D. Peroulis, "Tunable absorptive bandstop filter with an ultra-broad upper passband," in *IEEE MTT-S Int. Microw. Symp. Dig.*, Honolulu, HI, USA, 2017, pp. 1–4, to be published.

Mark D. Hickle (S'11–M'17) received the B.S. degree in electrical engineering from the Missouri University of Science and Technology, Rolla, MO, USA, in 2012, and the Ph.D. degree in electrical and computer engineering from Purdue University, West Lafayette, IN, USA, in 2016.

In 2017, he joined BAE Systems, Inc., Merrimack, NH, USA. He was a National Defense Science and Engineering Graduate Fellow with Purdue University.

Dr. Hickle was a co-recipient of the First Place Award of the RF-MEMS Tunable Filter Student Design Competition at the 2014 and 2015 IEEE MTT-S International Microwave Symposium and the First Place Award of the 2015 MTT-S Youtube/YouKu Video Competition.

Dimitrios Peroulis (S'99–M'04–SM'15–F'17) received the Ph.D. degree in electrical engineering from the University of Michigan, Ann Arbor, MI, USA, in 2003.

Since 2003, he has been with Purdue University, West Lafayette, IN, USA, where he is currently a Professor of electrical engineering and the Deputy Director of the Birck Nanotechnology Center. He has been a key contributor on developing high-quality reconfigurable filters and filter synthesis techniques based on tunable miniaturized high-Q resonators. He is also leading unique research efforts in high-power multifunctional RF electronics. He has co-authored over 300 journal and conference papers. His current research interests include reconfigurable electronics, RF MEMS, and sensors in harsh environment applications.

Dr. Peroulis was a recipient of the National Science Foundation CAREER Award in 2008 and the Outstanding Young Engineer Award of the IEEE Microwave Theory and Techniques Society in 2014. In 2012, he was the recipient of the Outstanding Paper Award from the IEEE Ultrasonics, Ferroelectrics, and Frequency Control Society (Ferroelectrics Section). His students have been the recipients of numerous Student Paper Awards and other student research-based scholarships. He is a Purdue University Faculty Scholar and has been the recipient of ten teaching awards including the 2010 HKN C. Holmes MacDonald Outstanding Teaching Award and the 2010 Charles B. Murphy award, which is Purdue University's highest undergraduate teaching honor.